RESEARCH ARTICLE

Module Lifetime Evaluation Method for the Power Converter of the DFIG Based on the Analysis of the Field Wind Speed Probability and Ambient Temperature

LE ZHANG[1] **AND JIADAN WEI**[2], (Senior Member, IEEE)

[1]Jiangsu International Cooperation Laboratory of 6G Network and Big Data Intelligent Application, Wuxi Taihu University, Wuxi 214064, China
[2]College of Automation Engineering, Nanjing University of Aeronautics and Astronautics, Nanjing 211106, China

Corresponding author: Le Zhang (zhangl1@wxu.edu.cn)

ABSTRACT The junction temperature fluctuation (ΔT_j) of the doubly fed induction generator (DFIG) around the synchronous speed point, deteriorates the reliability of the power converter considerably. Therefore, a lifetime evaluation method for the power converter of DFIG is proposed in this paper. Combining the speed-power curve of the generator with the grid side converter (GSC) and the rotor side converter (RSC), and using the equivalent thermo-electric network of IGBT module, the junction temperature (T_j) model of the power converter is established to calculate the average junction temperature and fundamental frequency temperature fluctuation. Based on the field measured data of the wind speed probability and ambient temperature of three wind power plants in different latitude region, the operation life curves of GSC and RSC are obtained by curve fitting, and the life spans of five type of power modules are evaluated and compared. Proved by the comparison that the lifetime of the converter could be reduced significantly due to the ambient temperature-induced low frequency temperature fluctuations in the thermal cycling, while, the fundamental frequency thermal cycle caused by the running frequency of the converter has slight effect on the overall life.

INDEX TERMS Junction temperature fluctuation, doubly fed induction generator, lifetime evaluation method, wind speed probability, power modules.

I. INTRODUCTION

With the increasing penetration of wind power plants in the power grid during the past few decades, the reliable and cost-effective wind energy production has become increasingly important [1], [2]. Due to its mature industry chain and low cost, DFIG is an attractive alternative for the MW-class power system of the wind turbines. As the key component of the electrical system, the power converter has relatively high cost and higher failure rates due to faults in the power components [3]–[5]. Shedding of the aluminum bonding wire and the thermal fatigue leading to the failure of the solder layer are

The associate editor coordinating the review of this manuscript and approving it for publication was Ehab Elsayed Elattar.

among the main causes of failure in the insulated gate bipolar transistor (IGBT) module. The accumulation of thermal stress caused by the fluctuation in the internal junction temperature of the IGBT is the root cause of these failures. The junction temperature of IGBT module is closely related to its packaging mode, chip type, layout, heat dissipation conditions and operating conditions. Specifically, for the DFIG operating around the synchronous speed point, the operation cycle of IGBT increases with the reduced fundamental frequency of the RSC output. This in turn increases the fluctuations in junction temperature, leading to the thermal stresses large in amplitude and alternating in nature. This alternating cycle of thermal stress at the junction between the layers of the chip accelerates the process of aging and failure [6]–[9].

Therefore, it is particularly important to develop a suitable method to correctly evaluate the DFIG converter's life expectancy while comparing the impact of different designs of power modules on the expected operational life.

In [10], [11], the influence of T_j and T_j on the lifetime of power devices is calculated to improve the traditional thermal electrical model of power devices. In [12], a comparison has been made of the power electronics lifetime for 5MW horizontal- and vertical-axis wind turbines, based on dynamic models supplied with generated wind speed time series. Literature in [13]–[16] depicts the lifetime evaluation of power devices considering the effect of change in wind speed and electrical loading conditions. In [17], DFIG wind turbine productivity was studied considering the electrical subassembly reliability. The control method with the loss distribution optimization of GSC and RSC is presented in [18] to improve the lifetime evaluation results of the power converter of wind turbine. A DFIG wind turbine based on the Matlab control model was established in [19], and the simulation verified that the lifetime of the RSC can be effectively improved by introducing a low-pass filter to the converter active power control loop. In [20], with improved control and paralleling devices, the positive impact of the reduced electrical stresses on the life expectancy of the GSC and RSC are comprehensively analyzed and demonstrated. A method for online real-time monitoring of the operation of a wind power generator is also provided in [21]. The parameters of power loss calculation, junction temperature data and online operation evaluation method for the lifetime evaluation of the power converter have attracted increasing attention in the wind power system.

In this paper, a model for the life-span evaluation of the power converter is established based on the site-specific wind turbine data to incorporate their effect on the thermal parameters of the wind turbine converter. Combining (a) the parameters of the wind turbine, (b) the site-specific ambient temperature, and (c) the wind speed probability curve at the installation site, the fatigue operational life curve of the converter is simulated and the lifespan of the converter is evaluated. It can provide a theoretical basis for the designation and selection of the power module for the wind turbine converter, and it is also valuable as abenchmark for the wind turbine operation and maintenance cycle evaluation.

The manuscript is organized as the following: In the section II, the electrical stresses of power converter for DFIG are analyzed, which includes the current and voltage stresses of GSC and RSC, as well as the fundamental frequency and the power factor. Then, in section III, the thermo-electric model of the converter is established to simulate the average temperature T_j and junction temperature fluctuation (ΔT_j) for the power converter. In section IV, the lifetime assessment model of the power converter is established, and the cycle life assessment of the wind power converter with the consideration of the five different power modules commonly used in the 2.2MW DFIG wind power system is carried out. The service life of the converter is also evaluated and verified

by the results of the measured parameters of wind plants in three geographically different and distant areas. Finally, the conclusion is drawn in section V.

II. OPERATING CURVE OF DFIG
A. OPERATING PRICIPLE OF POWER CONVERTER
Fig.1 shows the typical structure of a DFIG wind turbine [22]. Thedecoupling control for wind turbine of the DFIG generator is by two back-to-back three-phase converters. The RSC controls the excitation, output power, and output power factor of the generator. The GSC used for the constant DC bus voltage control and grid current harmonic control.
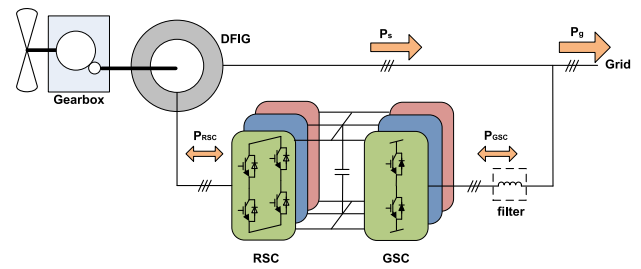

FIGURE 1. Schematic of the DFIG wind turbine system.

The power flowing of the DFIG wind turbine system can be shown as following.

$$P_g = P_s + P_{GSC} = P_s + P_{RSC} = P_s - sP_s \qquad (1)$$

where, P_g, P_{RSC}, P_{GSC} and P_s indicate the active powers of the grid port side, rotor side converter, grid side converter and stator side, respectively, s represents the slip frequency $(n_s - n)/n_s$ of the DFIG, which varies from -0.3 to 0.3 following the changes in the generator speed n.

The equivalent circuit diagram of DFIG is shown in Fig. 2 (a). The stator equivalent inductance, stator equivalent resistance, stator voltage, current, rotor equivalent inductance, rotor equivalent resistance, rotor voltage, current and excitation inductance are represented by X_{1_s}, R_{1_s}, $\overline{Us}$, $\overline{Is}$, R_{2_s}, X_{2_s}, $\overline{U'\mathrm{r}}$, $\overline{I'\mathrm{r}}$, X_m respectively. The relationship of rotor, stator voltage and current under super-synchronous mode and under synchronous mode are respectively shown in Fig. 2 (b) and Fig. 2 (c). Equations (2) and (3) can be obtained by solving the T-type equivalent diagram in Fig. 2 (a) and neglecting the equivalent resistance of stator and rotor, in which the polarity sign of s changes in the super-synchronous and under synchronous regions according to the change of generator speed. In Equation (3), σ is the leakage inductance coefficient which could be expressed as $X_{2\_s}(X_{1\_s}X_{2\_s} - X_m^2)/X_{1\_s}$.

$$\overline{I'_r} = -\frac{X_s}{X_m}I_{s\_Re} + jsign(s)(-\frac{U_{s\_Re}}{X_m} - \frac{X_s}{X_m}I_{s\_Im}) \qquad (2)$$

$$\overline{U'_r} = s(\frac{X_r}{X_m}U_{s\_Re} + \frac{\sigma X_r X_s}{X_m}I_{s\_Im}) - jsign(s)(s\frac{\sigma X_r X_s}{X_m}I_{s\_Re}) \qquad (3)$$
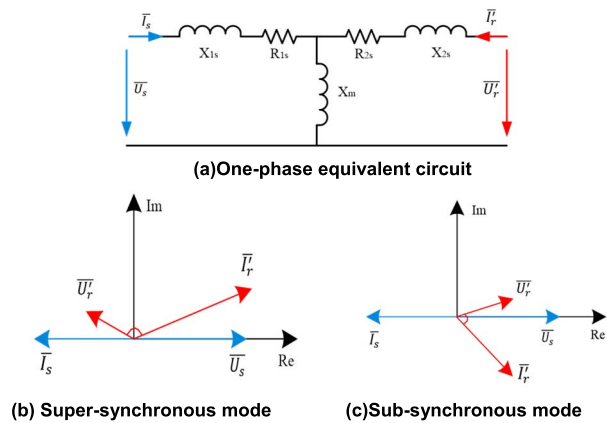
FIGURE 2. Phase vector diagram of the stator voltage, the stator current, the rotor voltage and the rotor current.

The equivalent circuit diagram of GSC as can be seen in Fig. 3 (a). X_g represents equivalent inductive reactance of the filter, $\overline{U}g$, $\overline{U}c$ and $\overline{I}g$ represent grid side voltage, converter side voltage and grid measured converter inductance current, respectively. The relationship between GSC voltage and current under two modes of super-synchronization and under-synchronization is can be seen from Fig. 3 (b) and Fig. 3 (c) respectively, as also shown in Equations (4) and (5).

$$\overline{I}_g = I_{g\_Re} + jI_{g\_Im} \tag{4}$$

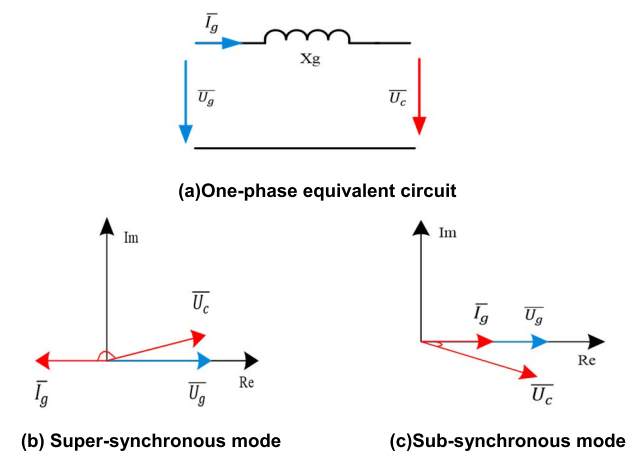$$\overline{U}_c = U_{g\_Re} - X_gI_{g\_Im} + j(-X_gI_{g\_Re}) \tag{5}$$

FIGURE 3. Phase diagram of the GSC output voltage and current.

B. OPERATING CURVE ANALYSIS OF DFIG

Tab.1 lists the parameters of a 2.2MW DFIG wind turbine and the electrical parameters of the generator equivalent circuit. Tab.2 shows the basic parameters of the corresponding DFIG converter. The converter adopts 2-level three-phase half bridge structure, and the GSC filter uses LC structure.

Fig. 4 shows the power curve and the generator speed curve of the wind turbine. The solid line is the power and wind

TABLE 1. Parameters of estimated DFIG wind turbine.

Parameters	Value
Wind turbine rated power （kW）	2250
Rated generator speed (r/min)	1680
Cut in wind speed (m/s)	3
Cut off wind speed (m/s)	25
Rated stator voltage(V)	690 line-line
Rated stator frequency (Hz)	50
Generator pole	4
Synchronous speed (r/min)	1500
Turns ratio Ns/Nr	0.373
Stator winding/Rotor winding	Δ/Y
Stator resistance $R1\_s$ (Ω)	0.00658
Stator leakage resistance $X1\_s$ (Ω)	0.03833
Magnetizing resistanceX_m(Ω)	2.3103
Rotor resistance $R2\_s$ (Ω)	0.00549
Rotor leakage resistance $X2\_s$ (Ω)	0.10088

TABLE 2. Parameters of estimated DFIG power converter.

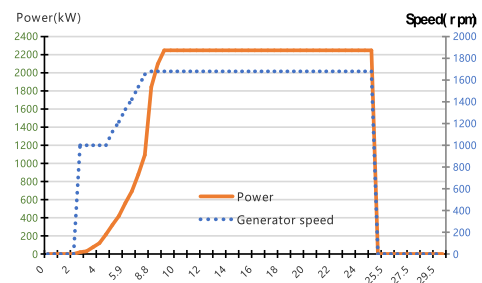| Parameters	Value
GSC and RSC topology	2 level half bridge
Grid-tied voltage (V)	690V line-line
DC link voltage U_{dc}(V)	1100
Filter inductanceL_g (mH)	0.35

FIGURE 4. Diagram of output power/generator speed vs wind speed of the 2.2MW wind turbine.

speed curve, and the dotted line is the generator speed and wind speed curve. It can be seen from Fig. 4 that the working wind speed range of the wind turbine is 3~25 m/s. When the wind speed is around 2.5m/s, the generator starts to idle, and the generator speed rises to 1000 rpm quickly, waiting for the wind power plant to be connected to the grid. In the wind speed range of 3~9.4 m/s, the wind turbine outputs the maximum power according to the wind speed power curve, and controls the generator speed to rise rapidly. When the wind speed reaches 9.4 m/s, the turbine reaches the rated power of 2.25 MW, and the rated speed of the generator goes up to 1680 rpm. The wind turbine maintains constant power output through the pitch control system, and maintains the generator speed as much constant as possible for the wind speed range of 9.4 ~25 m/s. The constant power and constant
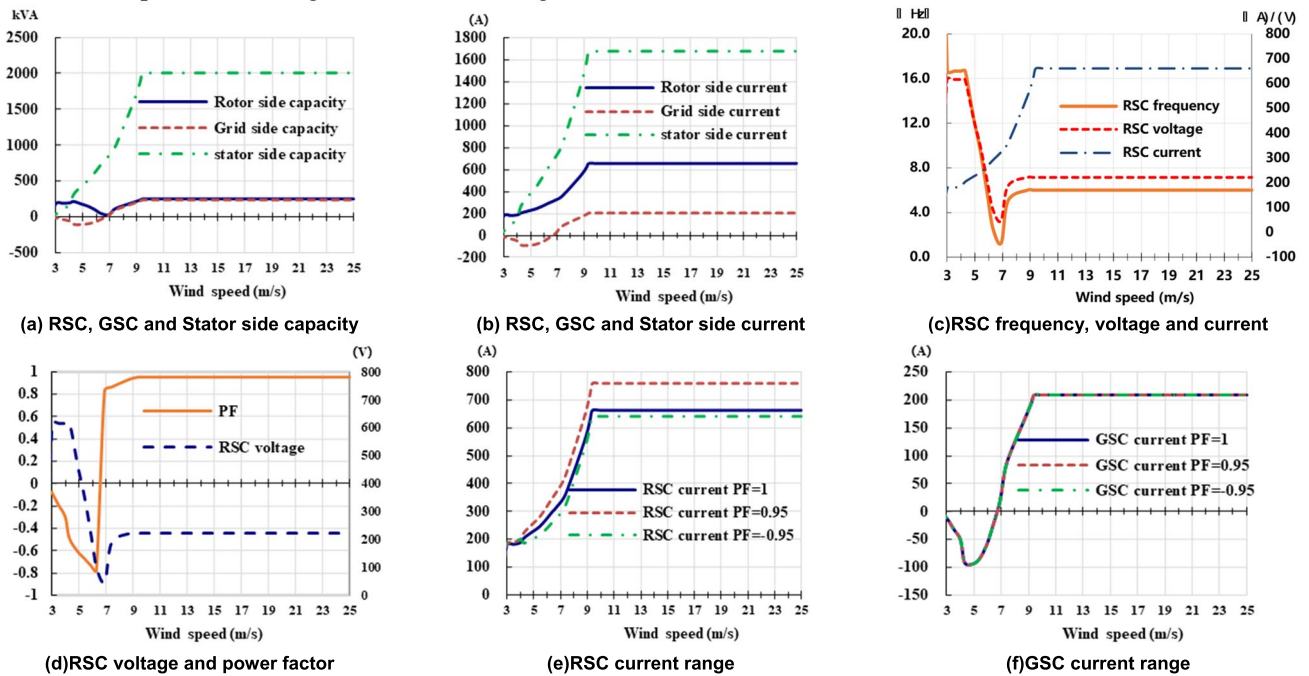
FIGURE 5. DFIG generator, GSC and RSC working curve.

speed characteristics can be managed until the wind speed stays up to the cut-off speed of 25 m/s. The wind turbine no longer remains in grid connected mode when the wind speed exceeds the cut-off speed and quickly stops by controlling the blade angles. As shown in Fig. 4, the generator works in sub-synchronous mode for the wind speeds from 3 m/s to 6.9 m/s. It runs in the synchronous mode for the wind speed of about 6.9 m/s and switches to super-synchronous mode for the wind speeds exceeding 6.9 m/s. The operation curves for the wind turbine, GSC and RSC can be traced based on equations (1) ~ (5) and using Fig. 4.

Fig. 5 (a) shows the power capacity curves of RSC side, GSC side and generator stator side. The power capacity of GSC and RSC named slip power, is only about $1/6^{th}$ of stator power capacity. Fig. 5 (b) shows the curves for current on rotor side, stator side and grid side. While the kVA capacities of RSC and GSC are almost the same, the working current of RSC is more than twice the current of GSC. Fig. 5 (c) shows the fundamental frequency, voltage and current curves on the RSC side. For the wind speed corresponding to the synchronous speed of the generator, the voltage and frequency of RSC reach their lowest points, close to zero. The current increases gradually with the wind speed until it reaches rated RSC current value. The fundamental frequency of RSC ranges from 0 to 16.7 Hz, which is much lower than the frequency of the parallel node as 50 Hz. Fig. 5 (d) shows the power factor and voltage curve of RSC. The power factor of RSC is: (a) negative for the wind speeds that correspond to less than the synchronous speed of the generator, (b) positive for the wind speeds that cause over synchronous speed, and this factor reaches maximum at the

rated working point. Fig. 5 (e) show the current curves of RSC at different power factors. The RSC current goes to a maximum of 780A with the condition of under excitation (0.95) power factor, which is the most severe operating point of RSC. RSC adjusts the stator output power factor of DFIG by controlling the excitation current. Fig. 5 (f) shows the current curve of GSC at different output power factors. GSC only plays a role in the stability of the DC link, rather than the regulation of system power factor. The wind speed current is negative before the synchronous speed, and reaches the maximum current of GSC at the rated wind speed. Since the GSC is always connected to the grid, the AC side voltage remains constant.

III. POWER LOSS ANALYSIS OF CONVERTER

The reliability of the converter is closely related to the junction temperature and its fluctuation. Therefore, to evaluate the reliability of the converter, it is necessary to establish its thermo-electric model. While the reliability evaluation model can be used to evaluate the reliability and life of the power devices, the junction temperature of the power devices can be derived by plugging in the actual converter loss in the model.

The thermo-electric model of power module consists of the device loss model and its thermal model. The loss model represents the characteristics of the power loss varying with voltage, current and temperature during the operation of the converter, while the thermal model represents the heat conduction characteristics of the path through which the power loss flows in the form of heat. The junction temperature value and junction temperature fluctuation of the device can be

directly simulated or calculated by the thermo-electric model to evaluate the converter lifetime.

The power module is composed of IGBT and diode in parallel. The power loss of IGBT and diode depend on the working mode of converter. The main loss components of IGBT are conduction loss and switching loss ($E_{on} + E_{off}$), whereas the losses in diode are mainly the conduction loss and reverse recovery loss. The conduction loss is primarily caused by the forward conduction voltage drop when the current passes through the IGBT or diode, which is positively related to the current. The switching loss is positively related to (a) the switching frequency of the converter, (b) the working voltage at both ends of the device and (c) the conduction working current. Equations (6) and (7) show the IGBT loss P_T and Diode loss P_D, respectively, taking phase A as an example.

$$P_T = \frac{U_{dc}}{U_{dc}^*} \left(\sum_{n=1}^{N} (E_{on}(|i_a(n)|) + E_{off}(|i_a(n)|)) \right)$$
$$+ \sum_{n=1}^{N} |i_a(n)| \cdot V_{ce}(|i_a(n)|) \qquad (6)$$

$$P_D = \frac{U_{dc}}{U_{dc}^*} \sum_{n=1}^{N} (E_{rr}(|i_a(n)|)) + \sum_{n=1}^{N} |i_a(n)| V_f(|i_a(n)|) \qquad (7)$$

where, U_{dc} and U_{dc}^* represent the actual working DC voltage and the loss measured DC voltage in the data sheet, respectively. N is the carrier ratio, whose value is the switching frequency over fundamental frequency, and subscript n is the nth switching pattern. E_{on}, E_{off} and E_{rr} represent the switching on loss, switching off loss, and diode reverse recovery loss of IGBT module, respectively. i_a is the sinusoidal current passthrough the IGBT and Diode. V_{ce} and V_f represent the connected voltage drop of IGBT and diode, respectively.

The converter capacity is usually less than 1/3 of the turbine power due to the converter of DFIG wind turbine only needs to deal with fraction of the turbine power, which results in the forced air-cooling method is often used for heat dissipation. Heat conduction can be observed between the materials in each layer of the IGBT power module, between the device and the heatsink, also between the heatsink and air. The thermal resistance model of IGBT with air cooling system is shown in Fig. 6.

The IGBT model adopts the fourth-order foster model [23], which consists of RC network in series through RC parallel connection. The thermal characteristic parameters of the four layers are named as $R_{thjc\_T1} \sim R_{thjc\_T4}$ and $t_{thjc\_T1} \sim t_{thjc\_T4}$ respectively, which can be obtained through the dynamic thermal impedance curve by experiment andthe RC value can be obtained by curve fitting. R_{th_CA1} is related to the TIM of IGBT module and heatsink, such as the material and thickness of silicone grease. R_{th_CA2} is the heat exchange resistance between the heatsink and outside air, which represents the cooling capacity of the radiator and cooling fan. It can be obtained by measurement or finite element simulation.
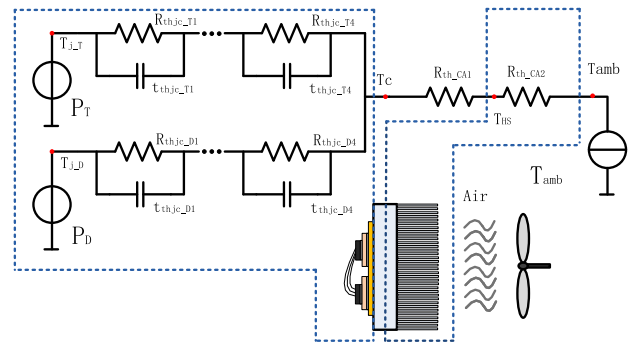

FIGURE 6. The Foster thermal modeling of air-cooling power modules.

In Fig.6, the model neglects the effects of heat radiation and heat convection while accounting for the heat conduction, so that the ambient temperature could be assumed as constant. Average junction temperature T_j of IGBT/Diode is named as $T_{j\_T/D}$ and shown in Equation (8).

$$T_{j\_T/D} = P_{T/D} \sum_{i=1}^{4} R_{thjc\_T/D(i)} + (P_T + P_D) \sum_{n=1}^{2} R_{thCA\_(i)} + T_{amb} \qquad (8)$$

where, $P_{T/D}$ represents the average power loss of IGBT/Diode which are calculated in equation (6) and (7), T_{amb} represents the ambient temperature.

The junction temperature ripple of IGBT/Diode is calculated as following.

$$\Delta T_{j\_T/D} = 2P_{T/D} \sum_{i=1}^{4} R_{thjc\_T/D(i)} \frac{(1 - e^{-\frac{t_{on}}{t_{thjc\_T/D(i)}}})^2}{1 - e^{-\frac{t_{cycle}}{t_{thjc\_T/D(i)}}}} \qquad (9)$$

where, t_{cycle} and t_{on} represent the fundamental period and loss duration of IGBT/Diode current, respectively. The time constant of the thermal resistance inside the device is far less than that in the external heatsink, thus the temperature of heatsink and device case is considered constant in calculating the junction temperature ripple of IGBT/Diode. For the 2-level half bridge circuit, the upper half bridge and lower half bridge devices work alternately during half period, so t_{on} is set as half of the fundamental period t_{cycle}.

IV. LIFETIME ASSESSMENT

The lifetime of the power module is the key factor affecting the overall lifetime of the converter. In the combination with the test data of the field anemometer tower, this section is based on the analysis of the power cycles of the power module to evaluate the power cycle lifetime of the converter. Based on the literature [24], the power cycle curve of Infineon's fourth generation IGBT chip is fitted by using the Coffin-Manson model. The fitting curve is shown in Fig.7, and the power
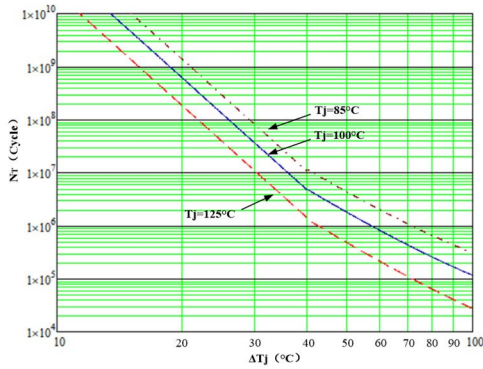
FIGURE 7. Fitting power cycle curve versus the junction temperature and the junction temperature ripple.

FIGURE 8. Flow chart of cycle life calculation.

cycle after fitting the curve Nt times is shown in formula (10).

$$Nt(T_j, \Delta T_j) = \begin{cases} K\Delta T_j^{\beta1} e^{\left(\frac{\beta2}{T_j+273}\right)} \cdot 0.083^{\beta3}, & \& 40 \geq \Delta T_j > 0 \\ K1\Delta T_j^{\beta4} e^{\left(\frac{\beta2}{T_j+273}\right)} \cdot 0.083^{\beta3}, & \& \Delta T_j > 40 \end{cases}$$
(10)

The coefficients in the formula are summarized in Tab. 3. The curve in Fig. 7 is fitted by the device manufacturers based on real measurement data [25]. It should be noted that the power cycle curve defined by Infineon refers to the device's thermal resistance which increases by 20% or the conduction voltage drop which increases by 5%. In this condition, the device can still operate normally with a failure rate less than 5%, which is different from the definition of device damage in practical application.

TABLE 3. Cycle number curve fitting parameters of Infineon fourth generation power devices.

Parameters	Value
K	1270000000
K1	1270000
β1	-5.039
β2	7166.7
β3	-0.463
β4	-5.351

While the junction temperature of the converter is a function of the working condition of the converter as well as the ambient temperature, the fluctuation in junction temperature on the other hand is only affected by the working condition of the converter. According to the wind speed data and the monthly average temperature measured by the anemometer tower installed in the early stage of the wind farm, the probability of different wind speed and the working ambient temperature of each month can be obtained. Then we can get the junction temperature fluctuation at different operating points, according to the calculation method in section 2 and section 3. After that, the power cycle number of the device
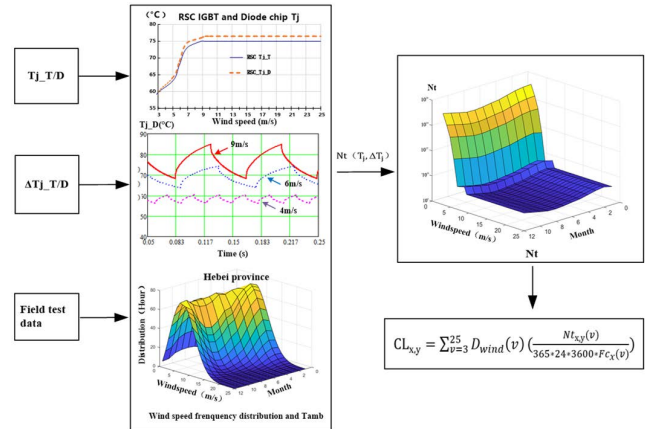
Nt can be obtained through equation (10). Considering the effect of working environment temperature, the Nt curve of wind speed probability characteristics is a 3D table. The lifetime expectancy calculation results of the device can be obtained by averaging all the calculated values in the 3D table according to the wind speed probability ratio, as shown in equation (11). The flow chart of lifetime evaluation is shown in Fig. 8.

$$CL_{x,y} = \sum_{v=3}^{25} D_{wind}(v)\left(\frac{Nt_{x,y}(v)}{365 \cdot 24 \cdot 3600 \cdot Fc_x(v)}\right)$$
(11)

where, x: RSC or GSC, y: T or D. $CL_{x,y}$ represents the cycle life of IGBT or Diode under different wind speed and probability ratio, its unit is year. $D_{wind}(v)$ is a function of wind speed probability ratio, which is the percentage of wind speed frequency $N_t(v)$ represents the total number of IGBT or Diode cycles under different wind speeds, and $Fc_x(v)$ represents the fundamental frequency of GSC or RSC under different wind speeds. Considering the working wind speed of the wind turbine is around 3~25m/s, only the cycle life within the working wind speed is need to be accumulated in the calculation of power cycle life.

The converter adopts three-phase system and uses multiple IGBT modules in parallel to increase the rated current of IGBT. Therefore, based on the formula (10), the IGBT life formula (12), the diode life formula (13), the grid side /rotor side converter life formula (14) and the whole wind turbine converter life formula (15) can be further derived.
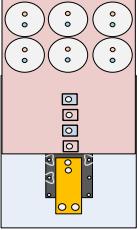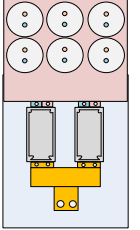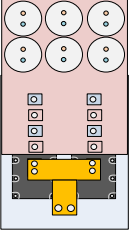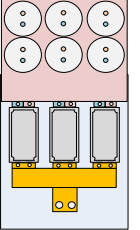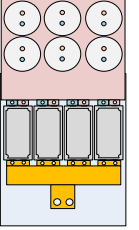
$$CL_{x\_T} = \frac{CL_{x,ST}}{3 \cdot N_{xp}}$$
(12)

$$CL_{x\_D} = \frac{CL_{x,SD}}{3 \cdot N_{xp}}$$
(13)

$$CL_x = \frac{1}{\frac{1}{CL_{x\_T}} + \frac{1}{CL_{x\_D}}}$$
(14)

$$CL_{Conv} = \frac{1}{\frac{1}{CL_{GSC}} + \frac{1}{CL_{RSC}}} \approx \frac{1}{CL_{RSC}}$$
(15)

TABLE 4. Parameters of the comparison phase leg power stack.

Power stack	PP1	ED2	PP2	ED3	ED4
Mechanical layout (one phase leg)					
Scenario	GSC	GSC	RSC	RSC	RSC
Current(A)	300	300	780	780	780
f_s(kHz)	3	3	2.5	2.5	2.5
Packaging	PrimePACK	EconoDUAL	PrimePACK	EconoDUAL	EconoDUAL
IGBT Type	FF1000R17IE4	FF600R17ME4	FF1000R17IE4	FF600R17ME4	FF600R17ME4
N_p	1	2	2	3	4
R_{th_jcT}(K/W)	0.024	0.037	0.024	0.037	0.037
R_{th_jcD}(K/W)	0.048	0.073	0.048	0.073	0.073
R_{th_CA1} (K/W)	0.00075	0.0086	0.00075	0.0086	0.0086
R_{th_CA2} (K/W)	0.01266	0.01266	0.01266	0.01266	0.01266
Tj_{max}(°C)	150°C				

where, CL_{conv} represents converter's cycle life value. CL_{x_ST}, CL_{x_SD} represent the cycle life values of single transistor IGBT and single transistor Diode, respectively. CL_{x_T}, CL_{x_D} represent the cycle life of all parallel IGBT and Diode in grid side and rotor side converters, respectively. N_{xp} represents the number of parallel IGBT modules in grid side and rotor side converters.

For the application of 2.2MW DFIG converter, 1700V half bridge IGBT modules are normally used to form phase leg power stacks with different current levels in parallel. The power cycle life of five power packages which consists of two IGBT modules FF600R17ME4 (EconoDUAL package) and FF1000R17IE4 (PrimePACK package) wasevaluated [25], [26]. There are two types of power kits for grid side converter, namely PP1(one phase grid side phase leg module is composed of single FF1000R17IE4) and ED2 (one phase grid side phase leg module is composed of two FF600R17ME in parallel).There are three types of power modules in the rotor side converter, namely PP2 (one phase rotor side phase leg module is composed of two FF1000R17IE4), ED3 (one phase rotor side phase leg module is composed of three FF600R17ME in parallel), ED4 (one phase rotor side phase leg module is composed of four FF600R17ME in parallel). Tomake all these modules are with the same structure and size, each of them uses the same heatsink and cooling fan, so they can be directly replaced. The parameters of each module are shown in Tab. 4.

The loss distribution of five power modules is shown in Fig. 9. Thepower loss represents only one power device from the power module. The loss of the whole phase leg power stack needs to be multiplied by the number of parallels. For the grid side converter in Fig. 9 (a) and (b), with the change of wind speed, the loss initially starts increasing with the wind speed. However, it peaks and starts decreasing. The loss

(a) PP1 loss (b) ED2 loss (c)PP2 loss (d)ED3 loss (e)ED4 loss
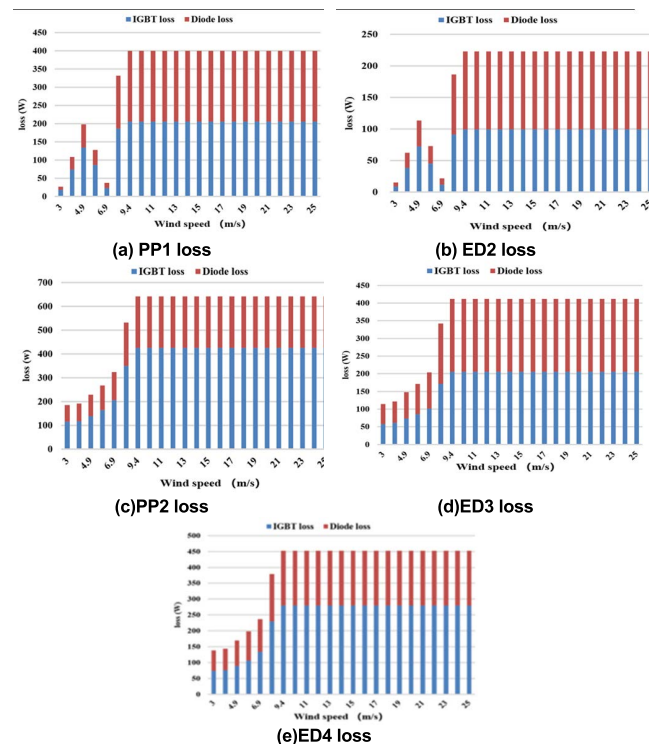
FIGURE 9. Loss breakdown of each GSC and RSC power stack device.

reaches its minimum values as the wind speed approaches the value corresponding to the synchronous speed of the generator. With further increase of wind speed and generator speed, the power loss reaches the maximum. As a result, the total power loss of ED2 module is greater than that of PP1. With the increase of wind speed and rotor speed, the power of the rotor side converter in Fig. 9 (c), (d), (e) increases
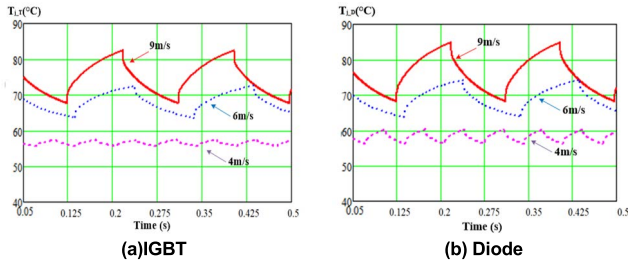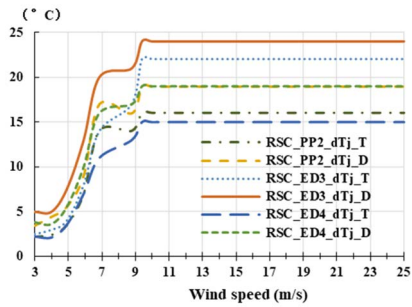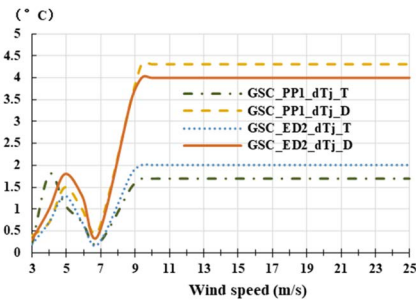
FIGURE 10. The simulation results of junction temperature ripple of RSC_PP2 power stack.

(a)RSC IGBT/ Diode chip △T

(b)GSC IGBT/ Diode chip △T

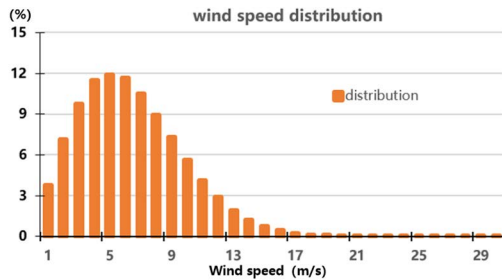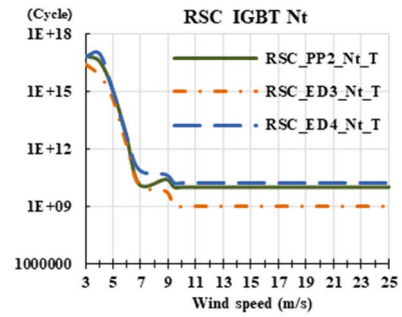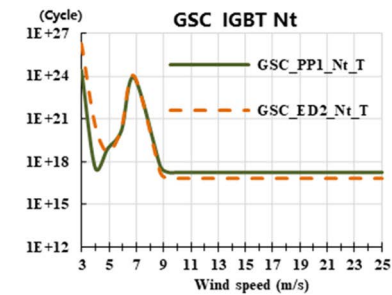**FIGURE 11.** Thermal profile comparison of each GSC and RSC power stack device.

FIGURE 12. Wind speed / frequency distribution curve of a wind farm.

(a) Comparison of IGBT/Diode cycle times of rotor side converter
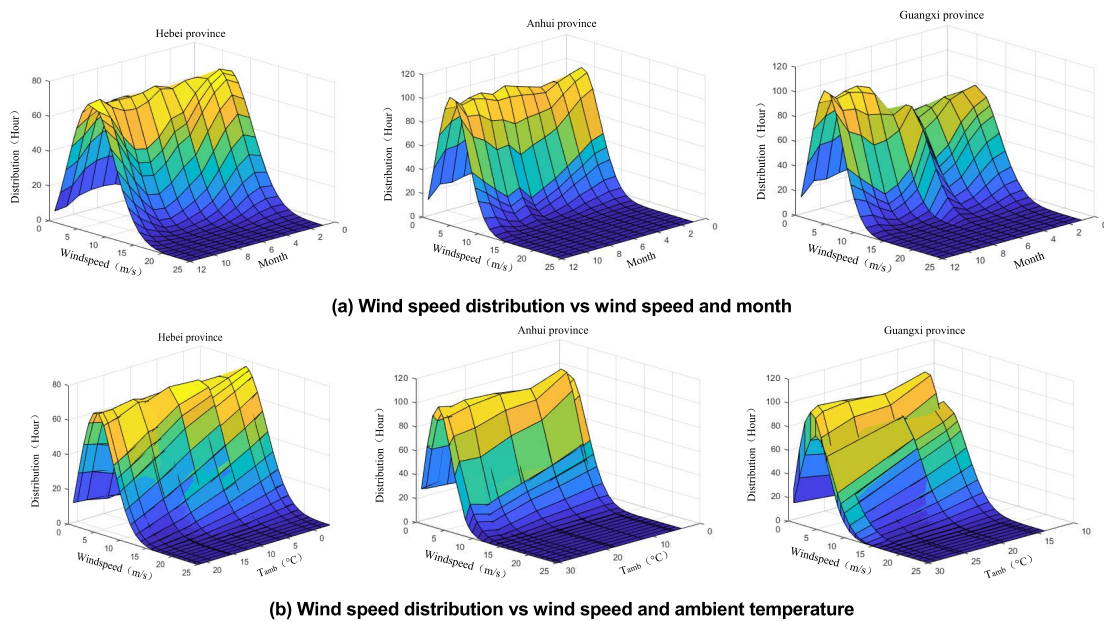

(b) Comparison of IGBT/Diode cycles of grid side converter

FIGURE 13. Cycle life comparison of IGBT and diode in grid side and rotor side converters.

and 6 Hz, respectively, the power at rotor side is 110 kW, 1830 kW and 2250 kW, respectively. It is also observed that the fundamental frequency changes with the increase of wind speed and power. The junction temperature and absolute temperature of IGBT/Diode significantly increase, and the junction temperature of Diode is slightly higher than that of the IGBT, which means that the junction temperature is noticeably influenced by the fundamental frequency.

Fig. 11 shows a comparison diagram of junction temperature of five power modules. The comparison of junction temperature ripple of three rotor side converter modules is shown

gradually, and the total loss shows trend as ED4 module >ED3 module > PP2 module.

Taking PP2 power module at rotor side converter as an example, the temperature fluctuation of IGBT and diode under different wind speeds is calculated in Fig. 10. When the wind speed is 4 m/s, 6 m/s and 9 m/s, the fundamental frequency of the converter on rotor side is 16.6 Hz, 5.6 Hz

(a) Wind speed distribution vs wind speed and month

(b) Wind speed distribution vs wind speed and ambient temperature

FIGURE 14. Wind speed, wind frequency, the month and temperature distribution of three wind farms.

in Fig. 11 (a), while the two grid side converter modules is in Fig. 11 (b). As can be seen, the ripple of grid side converter is much smaller than that of rotor side converter. The junction temperature ripple of IGBT devices on rotor side converter is ED3>PP2>ED4, and the junction temperature ripple of Diode shows like ED3>ED4>PP2. Because the most wind speed conditions correspond to the super-synchronous speeds for the wind turbine converter, the operating condition of the diode is worse. Meanwhile the thermal resistance parameters of Diode R_{thjc_D} is almost twice of that of IGBT R_{thjc_T}. Thus, the junction temperature ripple of Diode is much higher than that of the IGBT within the similar kind of module.

The wind speed probability ratio curve of a wind farm is shown in Fig. 12, in which the wind speed curve conforms to the Weibull distribution curve. The cycle number comparison of power module is calculated according to the Equation (10), as shown in Fig. 13. Due to the large numerical range of the data, the logarithmic coordinate axis is adopted. Comparing the results of Fig. 13 (a) and (b), we can have the below conclusions that the IGBT/Diode cycle life of GSC is several orders of magnitude longer than that of RSC., the influence of grid side converter on the overall converter cycle life is very small, and the he cycle capability of ED4 in RSC is very close to that of PP2 in IGBT / diode, which is much longer than that of ED3.

With a view to incorporate the effect of different climatic conditions of ambient temperature and wind speeds on life assessment of converters and to compare these, the following three wind farms at geographically different and distant sites were selected to carry out the life assessments of the above five converters: (1) Hebei Province in North China, (2) Anhui Province in Central China and (3) Guangxi

Province in South China. The wind speed frequency ratio characteristic curves of the three wind fields are shown in Fig. 14. The results show that the monthly wind frequency of Hebei wind field is relatively uniform, the characteristic of wind frequency curve is basically the same every month, and the proportion of high wind speed area from 9m/s to 13m/s is larger, while the monthly wind frequency of Guangxi wind field fluctuates greatly. In the months from August to December, the wind speed and frequency are higher, while in other months the wind speed and frequency are significantly lower, and that of Anhui wind field is somewhere in between, the wind speed area is mainly in 5m/s to 8m/s. The overall temperature of Hebei wind field is low, while the temperature of Guangxi and Anhui wind field is significantly higher. The high wind speed range of Hebei wind farm is concentrated with 0∼15°C, while that of Anhui and Guangxi wind farm is concentrated with 5∼13°C and 15∼25°C, respectively.

Fig. 15 shows the lifetime evaluation curves of single IGBT/Diode of three kinds of rotor side converter modules in different months. HB, AH, and GX in the figure represent the abbreviations of Hebei, Anhui and Guangxi wind fields, respectively. The trends of the life curves of several wind fields are similar for most parts, whereas the peak points of the individual trends are somewhat different due to the numerical difference in wind speed and ambient temperature data of the wind fields. In every month, the life cycle times of RSC diode are less than 2-3 times that of IGBT. The main reason is that the diode temperature ripple caused by the fundamental frequency is less than that of IGBT. Although the wind frequency characteristics of different months in different regions are quite different, the overall lifetime of the three months from May to September is lower than that
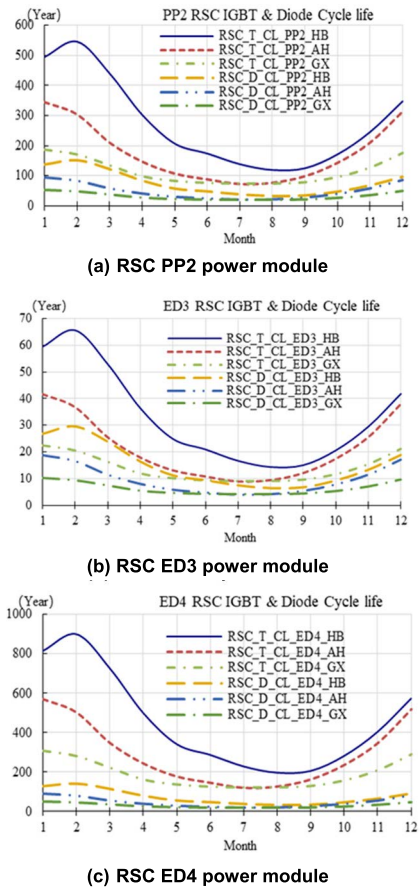
(a) RSC PP2 power module

(b) RSC ED3 power module

(c) RSC ED4 power module

FIGURE 15. Comparison of IGBT/Diode power cycle life of three RSC power modules in different wind fields.

FIGURE 16. Power cycle life comparison of RSC.

(a) GSC PP1 power module

(b) GSC ED2 power module

FIGURE 17. Power cycle life comparison of two different design GSC modules of wind farm with different installation.

of the other months, and GX<AH<HB, it is shown that the effect of low frequency temperature on the overall lifetime of the device is larger than that of RSC fundamental frequency caused by different wind frequency characteristics, and it is obvious that the cycle life of ED4>PP2>ED3 for single IGBT / diode.

The comparative results of the average lifetime of RSC converter are shown in Tab.5 and Fig. 16. Although the life of a single IGBT/Diode ED4 module is longer than that of PP2, considering the three-phase system and the total number of IGBT after parallel connection N_{igbt}, the life of power stack CL_{RSC} with PP2 structure is approximately twice that of ED4 structure, which is much longer than that of ED3 module, and has a good performance in the lifetime evaluation of various installation areas. Since the T_j of IGBT and Diode are only related to the power stack structure and wind turbine operating conditions, the cycle life difference between the various installation areas is only related to the local average operating ambient temperature. It can be inferred from the results of cycle life assessment of converters in Hebei and Guangxi Provinces that every time the ambient temperature rises by 10°C, the service life of electronic components will be dropped by half.
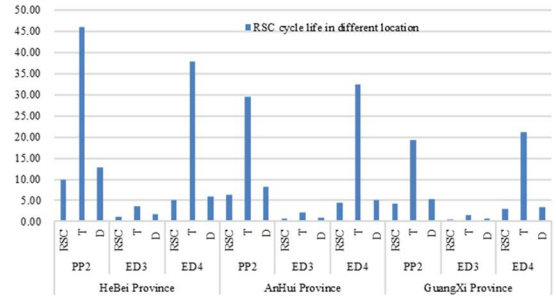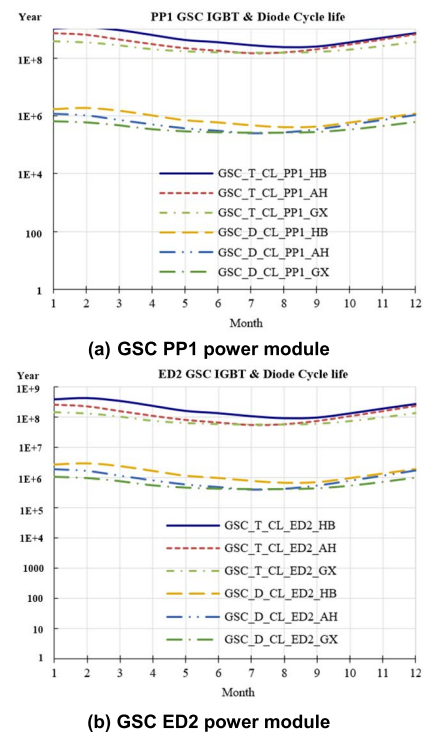
The lifetime evaluation curves of single IGBT/Diode of two types of rotor side converter modules in different months are presented in Fig. 17. The general trends of the life curves of several wind fields are overlapping for most parts, while the peak points of individual curves differ slightly due to variation in actual data of wind speed and ambient temperature in wind fields. It is obvious that for single IGBT, PP1 > ED2, and for Diode, ED2 > PP1. The unit of ordinate is year, which is expressed by logarithmic coordinate.

Fig. 18 show the comparison results of average life of GSC. The life of power stack with PP1 structure CL_{GSC} is approximately the same as that of the power stack with ED2 structure, which is much longer than the 30-year design life of the converter itself. So, they can meet the requirements of the converter life.

According to the above evaluation, the converter products with PP1 on grid side converter and PP2 on rotor side

TABLE 5. Power cycle life comparison of three RSC modules.

RSC module	PP2			ED3			ED4		
N_{igbt}	6			9			12		
Field location	He Bei	AnHui	GuangXi	HeBei	AnHui	GuangXi	HeBei	AnHui	GuangXi
CL_{RSC_ST}(Year)	276.02	176.96	115.37	33.16	19.77	13.20	454.96	291.73	190.24
CL_{RSC_SD}(Year)	76.59	49.28	32.26	14.94	8.93	5.99	71.94	46.36	30.4
CL_{RSC_T}(Year)	46.00	29.49	19.23	3.68	2.20	1.47	37.91	32.41	21.14
CL_{RSC_D}(Year)	12.76	8.21	5.38	1.66	0.99	0.67	5.99	5.15	3.38
CL_{RSC}(Year)	9.99	6.42	4.20	1.14	0.68	0.46	5.18	4.44	2.91
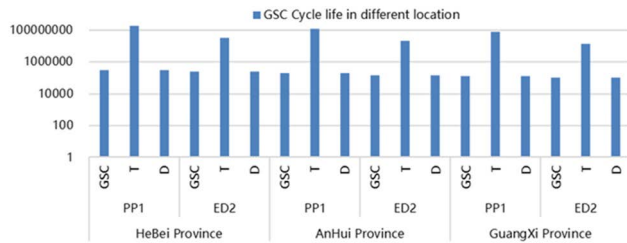
FIGURE 18. Power cycle life comparison of two different design modules of wind farm GSC with different installation.
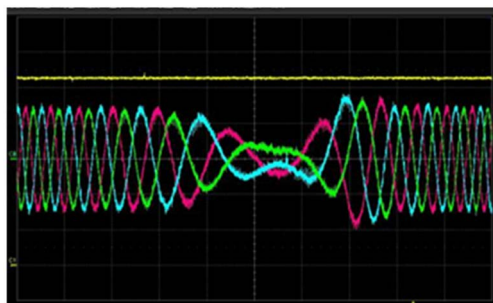
(a)   From sub-synchronous to super-synchronous speed
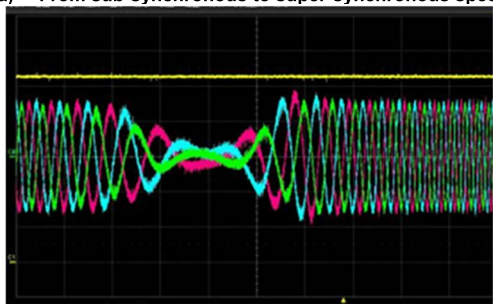
(b)   From super-synchronous to sub-synchronous speed

FIGURE 19. Experimental results for operation through the synchronous speed (C1: DC bus voltage(200V/div), C2-C4: RSC phase A, B, C current(200A/div)).

converter are applied to the experimental wind field, and the experimental waveforms are shown in Fig. 19. Fig. 19 (a) shows the waveform of speed ride through from sub synchronization to super synchronization, and Fig. 19 (b) shows the waveform of speed ride through from super synchronization to sub synchronization.

V. CONCLUSION
In this paper, a lifetime evaluation method for the power converter of DFIG based on the data analysis of wind speed

probability and temperature from wind power plant is proposed, and the cycle lifetime comparison of the power converters with the five different power modules are analyzed. The results showthatthe low frequency and high amplitude current of RSC lead to the higher junction temperature and short cycle life compared to the GSC, and the corresponding whole lifetime of power converter of DFIG is mainly determined by that of the RSC. With the same design of power loss and the heat dissipation, the low thermal resistance package and multi-device parallel connection of the power module significantly reduces the temperature fluctuation which not only increases the reliability but also improves the cycle lifetime of the power converter. Furthermore, the geographical site is also one of the important factors in the lifetime evaluation of the power converter. The mission profile of ambient temperature has a significant impact on the converterexpected lifetime due to low frequency thermal cycling, but not on the consumed lifetime due to the converter fundamental frequency thermal cycling. The proposed method also shows that a rise of 10°C in the mean annual temperature reduces the lifetime expectancy of the converter by as much as half.

REFERENCES
[1] F. Blaabjerg and K. Ma, "Future on power electronics for wind turbine systems," *IEEE J. Emerg. Sel. Topics Power Electron.*, vol. 1, no. 3, pp. 139–152, Sep. 2013.

[2] Q. Hui, J. Yang, X. Yang, Z. Chen, Y. Li, and Y. Teng, "A robust control strategy to improve transient stability for AC-DC interconnected power system with wind farms," *CSEE J. Power Energy Syst.*, vol. 5, no. 2, pp. 259–265, Jun. 2019.

[3] M. Shahbazi, P. Poure, and S. Saadate, "Real-time power switch fault diagnosis and fault-tolerant operation in a DFIG-based wind energy system," *Renew. Energy*, vol. 116, pp. 209–218, Feb. 2018.

[4] R. Moeini, P. Tricoli, H. Hemida, and C. Baniotopoulos, "Increasing the reliability of wind turbines using condition monitoring of semiconductor devices: A review," *IET Renew. Power Gener.*, vol. 12, no. 2, pp. 182–189, Feb. 2018, doi: 10.1049/iet-rpg.2017.0477.

[5] M. L. Hossain, A. Abu-Siada, S. M. Muyeen, M. M. Hasan, and M. M. Rahman, "Industrial IoT based condition monitoring for wind energy conversion system," *CSEE J. Power Energy Syst.*, vol. 7, no. 3, pp. 654–6644, May 2021.

[6] G. Breglio, A. Irace, E. Napoli, M. Riccio, and P. Spirito, "Experimental detection and numerical validation of different failure mechanisms in IGBTs during unclamped inductive switching," *IEEE Trans. Electron Devices*, vol. 60, no. 2, pp. 563–570, Feb. 2013.

[7] H. C. Yildirim, G. B. Marquis, and Z. Barsoum, "Fatigue assessment of high frequency mechanical impact (HFMI)-improved fillet welds by local approaches," *Int. J. Fatigue*, vol. 52, pp. 57–67, Jul. 2013.

[8] W. Lai, M. Chen, L. Ran, O. Alatise, S. Xu, and P. Mawby, "Low ΔT_j stress cycle effect in IGBT power module die-attach lifetime modeling," *IEEE Trans. Power Electron.*, vol. 31, no. 9, pp. 6575–6585, Sep. 2016.

[9] A. Morozumi, K. Yamada, T. Miyasaka, S. Sumi, and Y. Seki, "Reliability of power cycling for IGBT power semiconductor modules," *IEEE Trans. Ind. Appl.*, vol. 39, no. 3, pp. 665–671, May/Jun. 2003.

[10] W. Lai, M. Chen, L. Ran, S. Xu, H. Qin, O. Alatise, and P. A. Mawby, "Study on the lifetime characteristics of power modules under power cycling conditions," *IET Power Electron.*, vol. 9, no. 5, pp. 1045–1052, Apr. 2016.

[11] M. Ciappa, F. Carbognani, P. Cova, and W. Fichtner, "A novel thermomechanics-based lifetime prediction model for cycle fatigue failure mechanisms in power semiconductors," *Microelectron. Rel.*, vol. 42, nos. 9–11, pp. 1653–1658, Sep. 2002.

[12] M. A. Parker, C. Soraghan, and A. Giles, "Comparison of power electronics lifetime between vertical- and horizontal-axis wind turbines," *IET Renew. Power Gener.*, vol. 10, no. 5, pp. 679–686, 2016, doi: 10.1049/iet-rpg.2015.0352.

[13] Y. Qiu, W. Zhang, M. Cao, Y. Feng, and D. Infield, "An electro-thermal analysis of a variable-speed doubly-fed induction generator in a wind turbine," *Energies*, vol. 8, no. 5, pp. 3386–3402, Apr. 2015.

[14] K. Xie, Z. Jiang, and W. Li, "Effect of wind speed on wind turbine power converter reliability," *IEEE Trans. Energy Convers.*, vol. 27, no. 1, pp. 96–104, Mar. 2012.

[15] K. Ma, M. Liserre, F. Blaabjerg, and T. Kerekes, "Thermal loading and lifetime estimation for power device considering mission profiles in wind power converter," *IEEE Trans. Power Electron.*, vol. 30, no. 2, pp. 590–602, Feb. 2015.

[16] C. Li, Z. Tan, Q. Huang, W. Nie, and J. Yao, "Lifetime evaluation of IGBT module in DFIG considering wind turbulence and nonlinear damage accumulation effect," in *Proc. IEEE 2nd Int. Conf. Autom., Electron. Electr. Eng. (AUTEEE)*, Nov. 2019, pp. 472–476.

[17] H. Arabian-Hoseynabadi, H. Oraee, and P. J. Tavner, "Wind turbine productivity considering electrical subassembly reliability," *Renew. Energy*, vol. 35, no. 1, pp. 190–197, Jan. 2010.

[18] L. Wei, R. J. Kerkman, R. A. Lukaszewski, H. Lu, and Z. Yuan, "Analysis of IGBT power cycling capabilities used in doubly fed induction generator wind power system," *IEEE Trans. Ind. Appl.*, vol. 47, no. 4, pp. 1794–1801, Jul. 2011.

[19] L. Alhmoud, "Reliability improvement for a high-power IGBT in wind energy applications," *IEEE Trans. Ind. Electron.*, vol. 65, no. 9, pp. 7129–7137, Sep. 2018, doi: 10.1109/TIE.2018.2795568.

[20] F. Wani, U. Shipurkar, J. Dong, H. Polinder, A. J. Laguna, K. Mostafa, and G. Lavidas, "Lifetime analysis of IGBT power modules in passively cooled tidal turbine converters," *Energies*, vol. 13, no. 8, pp. 1875–1896, Apr. 2020.

[21] J. A. Baroudi, V. Dinavahi, and A. M. Knight, "A review of power converter topology for wind generators," *Renew. Energy*, vol. 32, pp. 2369–2385, Nov. 2007.

[22] Z. Wang and W. Qiao, "A physics-based improved cauer-type thermal equivalent circuit for IGBT modules," *IEEE Trans. Power Electron.*, vol. 31, no. 10, pp. 6781–6786, Oct. 2016.

[23] R. Bayerer, T. Herrmann, T. Licht, J. Lutz, and M. Feller, "Model for power cycling lifetime of IGBT modules-various factors influencing lifetime," in *Proc. 5th Int. Conf. Integr. Power Electron. Syst.*, Nuremberg, Germany, Mar. 2011, pp. 1–6.

[24] (Sep. 2020). *Infineon-AN2019-05_PC_and_TC_Diagrams-ApplicationNotes-v02_00-EN*. [Online]. Available: http://www.infineon.com/

[25] (Nov. 2016). *Datasheet FF600R17ME4 v3.0*. [Online]. Available: http://www.infineon.com/

[26] (Nov. 2013). *Datasheet FF1000R17IE4 v3.2*. [Online]. Available: http://www.infineon.com/

LE ZHANG received the B.S. and Ph.D. degrees in electrical engineering from the Nanjing University of Aeronautics and Astronautics (NUAA), Nanjing, China, in 2003 and 2014, respectively. From 2009 to 2015, he engaged in scientific research in government institutions. Since 2015, he has been a Faculty Member with Wuxi Taihu University. In 2019, he won the title of an Associate Professor. He has published 15 academic articles in journals and authorized eight national invention patents. His research interests include wind power generation, motor control, industrial informatization, and other fields, and has obtained the support of many government and enterprise funds.

JIADAN WEI (Senior Member, IEEE) received the B.S. and Ph.D. degrees in electrical engineering from the Nanjing University of Aeronautics and Astronautics (NUAA), Nanjing, China, in 2003 and 2009, respectively. Since 2009, he has been a Faculty Member at the Department of Electrical Engineering, NUAA, where he is currently a Full Professor with the College of Automation Engineering. From July 2016 to July 2017, he was a Visiting Scholar with the Power Electronics, Machine and Control (PEMC) Research Group, University of Nottingham. His research interests include new energy power conversion, power electronics, and machine control.

• • •